Investigation of Near Ohmic Behavior for Poly(3,4-ethylenedioxythiophene): A Model Consistent with Systematic Variations in Polymerization Conditions

Yohani P. Kayinamura,[†] Marc Ovadia,[‡] Daniel Zavitz,[§] and J. Faye Rubinson*[,†]

Department of Chemistry, Georgetown University, 37th and O Streets, NW, Washington, D.C. 20057, College of Engineering, The University of Illinois, Chicago, Illinois 60607, and Department of Chemistry, University of Illinois, Chicago, Illinois 60607

ABSTRACT The impedance behavior of semiconducting polymer film electrodes based on poly(3,4-ethylenedioxythiophene) (PEDOT) in combination with a series of anionic dopants has been investigated using electrochemical impedance spectroscopy (EIS) over the frequency range from 0.1 Hz to 100 kHz. Films were electrodeposited on gold-coated Pt wire electrodes from a nonaqueous solution containing 3,4-ethylenedioxythiophene (EDOT). EIS results reveal that, under the optimal synthesis conditions, PEDOT electrodes consistently exhibit low, frequency-independent impedance over a wide frequency range (from ~10 Hz to 100 kHz). These results suggest that the behavior originates from the two-layer homogeneous morphology of the film. A model for conduction in the films that is supported by experimental evidence is proposed, and EIS data for electrodes produced under a variety of electropolymerization conditions are presented.

KEYWORDS: Conducting polymer • impedance spectroscopy • charge transport • PEDOT • sensing

1. INTRODUCTION

The solid electrodes presently used for monitoring biosignals, such as Pt, Au, and Ag/AgCl (1−3), typically exhibit high-pass frequency filtering behavior because of their diffusional and interfacial double-layer capacitive behavior. As conducting polymers, in particular, poly(3,4-ethylenedioxythiophene) and polypyrrole have already been shown to be potential candidates for the development of implantable bioelectrodes because of their stable electrical properties and biocompatibility (4−6), these electrodes present a logical category of candidates for investigation.

The results reported here focus primarily on the development of electrodes that exhibit frequency-independent behavior in the regime relevant to biological signals (<1000 Hz), particularly in the range between 1 and 50 Hz. This range is of critical importance for detection of signals associated with movement disorders. A second aspect of the studies reported here is the relationship between electrochemical properties of conducting polymers and their mesoscopic morphological features. Although such investigations have been reported for many years, there still is a need for a unified concept establishing links between the morphological features and a specific electrochemical property resulting from optimization of synthetic approaches.

Poly(3,4-ethylenedioxythiophene) (PEDOT) has attracted considerable interest because of its electrochemical stability (7, 8). When used as an electrode coating in asymmetric configuration (metal−film−solution), the PEDOT film forms a heterogeneous interface with its surroundings. Previous investigators have reported that PEDOT electrodes in such configurations exhibit frequency-dependent impedance behavior and have explained its behavior on the basis of an equivalent circuit containing a combination of capacitive, diffusional, and resistive elements (9). Such frequency-dependent behavior can be problematic for biosensing applications that require reliable recording of low-amplitude signals at low frequencies (10). For example, performance of a sensing/pacing pacemaker relies on both stimulation and sensing cycles. The sensing electrode must be able to report low-amplitude heartbeat signals that occur at low frequencies. The high-pass frequency filtering behavior of electrodes currently in use presents the possibility that the signals may be attenuated in a manner that depends on signal frequency and interfacial transfer function (2). A sensitive probe for the likelihood of such problems is found in the imaginary component of the interfacial impedance behavior at low frequencies (11).

Whether films are spin-cast from polystyrene sulfonate (PSS^-)-doped PEDOT (12) to form lamellae of alternating PSS^- and PEDOT regions or electrodeposited from solutions of monomer in salts of PSS^- or small anions such as chloride

* To whom correspondence should be addressed: Department of Chemistry, Georgetown University, Box 571227, 37th and O Streets, NW, Washington, DC 20057. E-mail: jfr@georgetown.edu. Phone: (202) 687-2066. Fax: (202) 687-6209.

Received for review June 2, 2010 and accepted August 1, 2010

[†] Georgetown University.

[‡] College of Engineering, The University of Illinois.

[§] Department of Chemistry, University of Illinois.

DOI: 10.1021/am100480s

(9, 13), to form fibrous networks or "cauliflower" aggregations, the morphology of the film generally is not uniform on a nanoscopic or even microscopic level. This means that electrons (or holes, h^+) must traverse regions of low conductivity between the PEDOT-heavy areas and that anions from solution can diffuse in and out. The capacitance due to the latter is particularly important at low frequencies. For example, Xiao et al. (14) have reported that the impedances of the films produced from PEDOT doped with its derivative sulfonatoalkoxy EDOT (S-EDOT) are on the order of 10 kΩ at 1 kHz and tend to become even higher at lower frequencies.

We recently reported frequency-independent behavior for tosylate-doped PEDOT bioelectrodes in the frequency range of 25−806 Hz (15). Herein we report an efficient and practical method for reproducibly electrosynthesizing electrodes based on PEDOT doped with other anions that exhibit such ohmic behavior in solution studies with a low overall impedance and outline polymerization conditions that extend that behavior to lower frequencies. The optimization has been accomplished through a systematic adjustment and screening of morphological features and interfacial transfer function characteristics and through the choice of suitable electropolymerization conditions and dopant (16). These systematic studies also have provided the necessary information for the development of a model for conduction in these films. When these studies are correlated with those for in vivo studies (17), a clear link will allow prescreening of new conducting polymer electrode types before in vivo characterization is conducted, thus reducing the number of animal, or human, subjects required for a comprehensive evaluation.

2. EXPERIMENTAL SECTION

Materials. Platinum (Puratronic grade) and silver (99.99%) wires, as well as hydrogen tetrachloraurate(III), were purchased from Alfa-Aesar. Sulfuric acid, potassium chloride, potassium ferrocyanide, and acetonitrile (99.9%) were purchased from Fisher Scientific. The EDOT monomer, 3,4-ethylenedioxythiophene, was obtained from Aldrich. Tetrabutylammonium tetrafluoroborate, tetrabutylammonium hexafluorophosphate, poly(sodium 4-styrenesulfonate) (PSS), sodium *p*-toluene sulfonate (TS^-), and lithium perchlorate (electrochemical grade) were obtained from Fluka Chemika or Aldrich. Acetonitrile was dried over 3 Å molecular sieves (Fisher Scientific) before use. All other chemicals were used without further purification. Adhesive polymer was obtained from Stan Rubenstein Associates (Foxboro, MA) or M. E. Taylor Engineering, Inc. (Brookeville, MD). Nonporous polymer (TorrSeal) was purchased from Varian Vacuum, Inc. Aqueous solutions were prepared using 18.3 MΩ cm^{-1} water produced with a Millipore RIOS purification system.

Electrodeposition and Electrochemical Characterization. All electrodepositions [with the exception of a flow deposition conducted using a published procedure (18)] and electrochemical characterization studies were conducted in a one-compartment, three-electrode glass cell. The reference and auxiliary electrodes were Ag/AgCl (BAS RE5) and platinum wire, respectively. Studies were performed using a Radiometer PGZ402 instrument controlled with VoltaMaster 4. No ohmic compensation has been applied. EIS data shown herein were acquired at an open circuit potential in 0.1 M KCl.

Raman Characterization. Raman measurements were taken by employing a Renishaw Ramascope instrument equipped with a 25 mW 785 nm laser (SpectraPhysics), a Rayleigh filter, and a 1200 line/mm grating. The instrument was interfaced with an Olympus BH-2 microscope, and data acquisition was controlled using Wire 2.0. Peak intensities used for determination of the doping level were based on the intensities reported by Wire 2.0. Spectra were recorded under ambient conditions on samples prepared in the same manner described below for the working electrodes used for the EIS studies, and spectra were obtained from at least two areas of the film for each sample to verify homogeneity across the film.

SEM Characterization. Samples of polymer-modified wires (prepared using the same manner described below for the working electrodes used for the EIS studies) were cut and placed onto circular adhesive carbon films to be affixed to aluminum sample stubs. The electron micrographs were collected using a Zeiss Ultra Plus Field Emission scanning electron microscope with an operating voltage range of 1−5 kV under ultrahigh vacuum conditions. All images were captured using SmartSEM Ultra Plus.

Preparation of Working Electrodes. Each electrode was fabricated by attaching a 250 μm diameter × 2 cm Pt wire to a 250 μm diameter × 10 cm Ag wire via conductive silver epoxy. The Ag/Pt junction area was housed in a short glass tube (approximately 8 cm long), and a nonporous polymer was applied at the exit of the working electrode from the glass tube to prevent any contact of the liquid with the junction. The conductive epoxy and masking polymer were each allowed to cure for 24 h before the next step was undertaken.

Each electrode was electrochemically cleaned to ensure adhesion of the film, using the following sequence: −0.2 V in 5 M NaOH for 15 min, 1.4 V for 10 min in 1 M H_2SO_4, 0.2 V for 30 s, and twenty cycles between −0.2 and 1.2 V in 1.0 M H_2SO_4 at a scan rate of 100 mV/s. The solution was purged with N_2 prior to, and blanketed with N_2 during, each step. The acid and base solutions were changed every after every five electrodes, and each electrode was rinsed with deionized H_2O between steps.

In this investigation, a polycrystalline gold layer was electrodeposited before polymer deposition to improve film adhesion (13). The plating process was allowed to run for 1 min (until approximately 100 mC had passed) at a constant potential of 0.3 V versus Ag/AgCl in 50 mM $HAuCl_4$ prepared in 0.1 M NaCl. The solution was changed between every five electrodes and was deaerated with N_2 prior to, and blanketed with N_2 during, the plating process.

The PEDOT films were electrodeposited potentiostatically (1300 mV vs Ag/AgCl) from an acetonitrile solution containing the monomer and a background electrolyte, the anion of which acts as the dopant. The electropolymerization time was varied between 30 and 120 s to produce films with a thickness of 1.1−2.4 μm, as measured by SEM and/or charge transferred during deposition. The thickness was based on eq 1

$$d = \frac{(\mu + px)q}{(2 + p)F\rho} \tag{1}$$

where d is the thickness, μ is the molar mass of the monomer, p is the doping level, x is the molar mass of the counterion, q if the charge passed during deposition, F is Faraday's constant, and ρ is the density of the polymer (19). (The doping level and density are the terms that are likely to introduce the greatest error into the approximation.) A typical plot of charge passed versus time is shown in Figure 1.

The concentration of the monomer (EDOT) and the identity and concentration of the background electrolyte were varied as described in Results and Discussion. The films were characterized using SEM, impedance spectroscopy, cyclic voltammetry, and Raman spectroscopy, and the lower limit of the

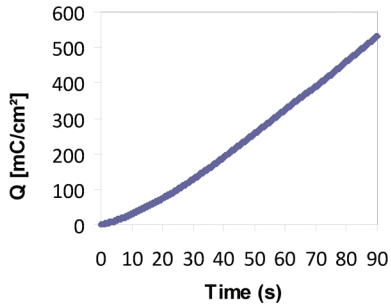

FIGURE 1. Typical deposition curve in 0.0125 M EDOT and 0.1 M TBATFB. $V = 1.3$ V vs Ag/AgCl.

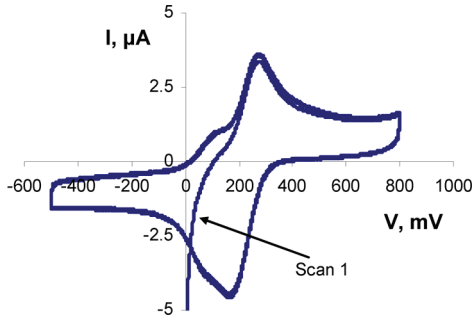

FIGURE 2. Cyclic voltammogram of 0.010 M $Fe(CN)_6^{3-/4-}$ at the PEDOT/BF_4 electrode (supporting electrolyte, 0.1 M KCl).

frequency-independent range of impedance was the primary optimization criterion.

3. RESULTS AND DISCUSSION

Characterization of Electrodes by Cyclic Voltammetry. Cyclic voltammetry (CV) was used to investigate stability and to screen for the possibility of overoxidation of PEDOT films. Such overoxidation has been reported to result in the production of sulfoxide moieties in the film and a decrease in conductivity and stability (7, 20). Electrodes prepared as described above exhibited reversible electrochemical behavior for ferricyanide before and after EIS experiments. Figure 2 shows a CV of 0.01 M $Fe(CN)_6^{3-/4-}$/0.1 M KCl at PEDOT/BF_4^- produced under the optimal conditions discussed below. Two cathodic and anodic peaks are observed. While the main (larger) peaks, separated by approximately 85 mV, can be attributed to the solution redox reaction of $Fe(CN)_6^{3-/4-}$, the origin of the shoulders on these peaks is unclear at this time. It is possible that these may derive from the redox reaction of $Fe(CN)_6^{3-/4-}$ that is adsorbed or incorporated as the dopant at the inner pore walls. This ferri/ferrocyanide couple may be characterized by a potential that is slightly different from that at the film–solution interface. This suggestion of an immobilized redox couple is supported by the near superposition of the peak potentials and the absence of this peak in CVs of control samples: $Fe(CN)_6^{3-/4-}$ at a PEDOT/PSS^- electrode (which, as reported below, is almost pore-free), $Fe(CN)_6^{3-/4-}$ at Pt electrodes, and scans at PEDOT/BF_4^- in the background electrolyte only. The voltammograms exhibit steady state behavior beginning with the second scan, and the stability of the film was verified by monitoring charge transferred during the anodic and cathodic processes for the electrode in the background electrolyte. We attribute the capacitive current background to double-layer charging (21).

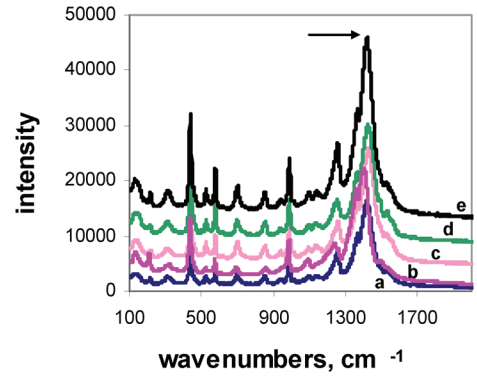

FIGURE 3. Raman spectra for PEDOT doped with various counterions: (a) poly(styrene sulfonate), (b) *p*-toluene sulfonate, (c) hexafluorophosphate, (d) perchlorate, and (e) tetrafluoroborate. All films were prepared at a constant potential chosen to prevent overoxidation. Solution conditions: 0.0125 M monomer and 0.1 M ammonium (for TFB, HFP, and ClO_4^-) or sodium (for PSS^- and TS^-) salt of dopant in acetonitrile.

Table 1. Doping Levels of PEDOT Polymers Used in This Study

counterion		estimated doping level	ionic radius (nm) (38)
hexafluorophosphate	PF_6^-	31.6	0.254
perchlorate	ClO_4^-	31.3	0.237
tetrafluoroborate	BF_4^-	35.2	0.229
p-toluene sulfonate	TS^-	28.4	–
polystyrene sulfonate	PSS^-	26.1	–

Characterization of Electrodes by Raman Spectroscopy. Raman spectroscopy has been used to verify that the films are not overoxidized. All electrodes investigated exhibit structural vibration modes typical for PEDOT, as seen in Figure 3. The maximum for $C_\alpha{=}C_\beta$ absorption resulting from the doped, oxidized polymer is located at or around 1432 cm^{-1}, while that for the asymmetric vibration of $C_\alpha{=}C_\beta$ bond associated with the neutral (reduced) form appears at approximately 1412 cm^{-1}. The ratio of the peak intensities at these two positions can be used to estimate the dopant ratio in the polymer, y, based on eq 2, where I is the natural logarithm of the peak ratio (22).

$$I = 0.087y - 2.279 \quad (2)$$

The results for typical electrodes are listed in Table 1. All values were in the normal range of one dopant for every three or four sites (23), and none of the polymers exhibit the S=O stretch that would be characteristic of sulfoxide groups present in the overoxidized form (which would appear at approximately 1320 cm^{-1}) (24). The low impedances (described below), the typical doping levels, the smooth increase in the charge versus time curve during deposition, and the absence of an S=O vibration in the Raman spectrum suggest that the polymers produced using the methods described are not overoxidized.

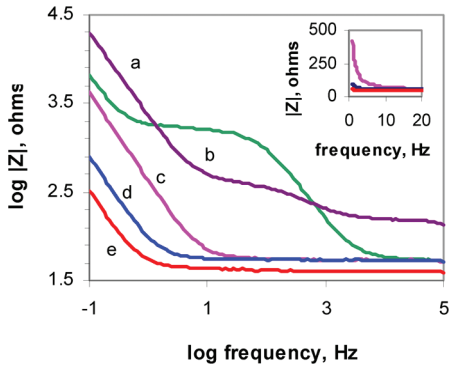

FIGURE 4. Bode plot for electrodes prepared with varying counterions: (a) poly(styrene ulfonate), (b) *p*-toluene sulfonate, (c) hexafluorophosphate, (d) perchlorate, and (e) tetrafluoroborate. The inset shows behavior at a low frequency between 1 and 25 Hz for the last three dopants. All films were prepared at a constant potential chosen to prevent overoxidation. Solution conditions: 0.0125 M monomer and 0.1 M ammonium (for TFB, HFP, and ClO_4^-) or sodium (for PSS^- and TS^-) salt of dopant in acetonitrile. $t_{dep} = 60$ s.

EIS Characterization of Electrodes. Figure 4 shows the impedance magnitude, $|Z|$, of PEDOT electrodes doped with ClO_4^-, PSS^-, BF_4^-, TS^-, and PF_6^- as a function of frequency prepared using the same electrochemical and solution compositions (other than dopant identity). PEDOT/PSS^- and PEDOT/TS^- electrodes clearly exhibit the highest, frequency-dependent impedance through the frequency range shown. Though the impedances of PEDOT doped with the inorganic anions are more comparable in magnitude, PEDOT/BF_4^- is clearly distinguished by a slightly lower impedance magnitude and frequency-independent behavior over a broader frequency range. In general, PEDOT films prepared as described above with smaller anionic background electrolytes than PSS^-, or even its monomer *p*-toluene sulfonate, exhibit near ohmic behavior at frequencies as low as 1−10 Hz, which is unusual for polymer-modified electrodes. The sizes of the inorganic ions appear in Table 1. Although they vary widely in size, these ions all can be envisioned as possessing a spherical distribution of charge. Toluene sulfonate and PSS^-, however, tend to interact with the monomer through π interactions. The order imposed by the anions results in a templating effect similar to that described by Laforgue and Robitaille (25) and results in alternating areas of polymer and dopant. In addition to the expected difference in the dopant distribution in the film, it is also worth noting that doping with PSS^- would result in "extra" anionic sites which could trap the h^+ carriers and alter charge transport behavior (26).

The range over which the impedance was frequency-independent for the PEDOT/BF_4^- electrodes was, as described below, sensitive to electrodeposition parameters. However, when fabricated using the optimal conditions, the high-frequency impedance modulus of 50 Ω (a function of the IR drop across the Ag/AgCl reference electrode and the solution resistance during the EIS measurements) and the low-frequency cutoff for constant, non-frequency-dependent impedance (phase angle of less than ±2°) were both consistent electrode to electrode.

It is generally agreed that the external surfaces of conducting polymer films are porous. This follows from their growth mechanism, which involves a two-dimensional (2D) nucleation growth followed by a three-dimensional growth (27, 28). The initial 2D nucleation growth results in the complete coverage of the substrate by a homogeneously compact layer. Subsequent growth leads to the formation of a porous, noncompact layer on the top of the compact layer (29). Solvent, counterion type, and deposition rate and mode affect the morphology and quality of the film (29), as all of these impact the kinetics of these growth steps.

Morphology Studies by SEM. SEM images (Figure 5) provide concrete evidence of the proposed morphological model shown in Figure 6. Panels a−d of Figure 5 show the surfaces of a series of electrodes prepared using difference electrodeposition times. In Figure 5a, the early stages of nucleation (7 s) can be seen, while Figure 5b shows the outer surface of the film after electropolymerization for 30 s. It is obvious that growth from the initial nucleation sites has begun to form compact structures. The 30 s electrode also exhibits a more compact surface structure and a smoother surface morphology compared to those of a film produced over a 90 s electropolymerization period (Figure 5c).

The increase in film porosity with an increase in thickness is also illustrated in Figure 5d. The film was produced by partially immersing the wire in the electropolymerization solution and raising a part of it above the solution after 45 s. The bottom portion of the electrode was left in the solution to allow additional polymerization for an additional 75 s. The portion formed at longer polymerization times is seen to be much more porous and the structure seems more compact near the underlying metal substrate.

The more compact nature of the sample film at the metal−film interface is also evident in panels e and f of Figure 5. In Figure 5e, the outer surface is clearly much more porous than the inner layers. In Figure 5f, the sample film was removed (with a carbon adhesive used for SEM studies) to look at the side of the film adjacent to the deposition electrode. The metal−film surface is seen to be compact and smooth. The gaps where portions of the film adhered to the surface of the electrode during removal show that the film is porous toward the outside (circles area). The presence of these gaps also attests to the difficulty in removing the film from the surface, an additional desirable property.

This postulated requirement for a two-layer morphology, which is proposed below to be the origin of the observed ohmic behavior, is further supported by the morphology of the PEDOT/PSS^- film shown in Figure 5g. Zooming in on a crack and looking at the film's surface show that, unlike the PEDOT/BF_4^- film, this film is homogeneously compact. Its outer surface can be described as rough instead of porous. While PEDOT/BF_4^- exhibits ohmic behavior, PEDOT/PSS^- lacks an ohmic signature in the frequency range of interest.

Charge Transport Model for a Two-Layer Film. The presence of two distinct layers presents an interesting question in terms of predictions of impedance behavior. A morphological model consisting of two different macro-

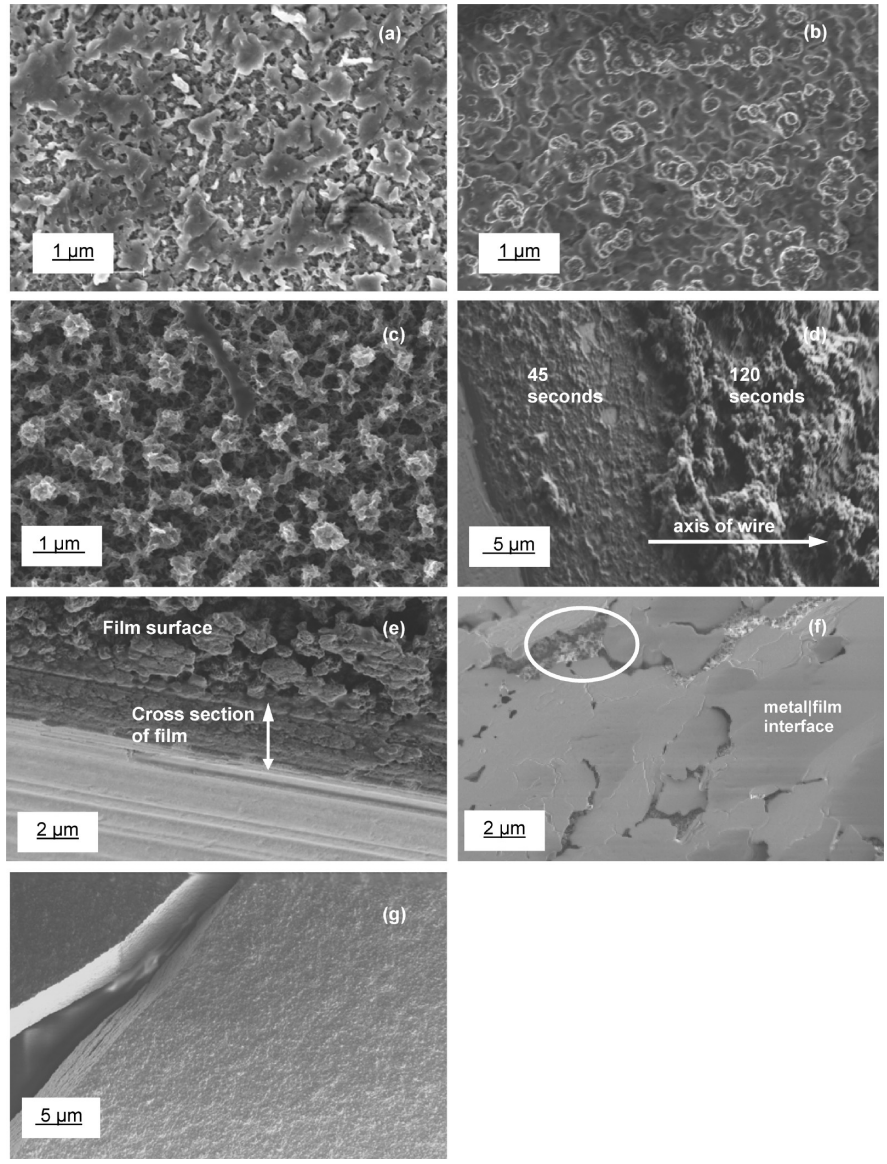

FIGURE 5. SEM images showing the morphology of the PEDOT/BF_4^- film. Electropolymerized film after (a) 7, (b) 30, (c) 90, and (d) 45 and 120 s at the deposition potential. (e) Cross section of PEDOT/BF_4^-. t_{dep} = 120 s. (f) Polymer morphology at the metal−polymer interface. t_{dep} = 120 s. (g) Surface morphology of PEDOT/PSS^-. t_{dep} = 60 s.

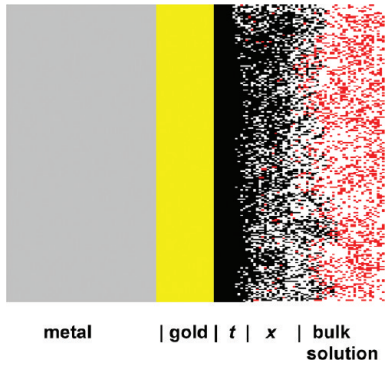

FIGURE 6. Morphological model of a PEDOT film. *t* is the compact layer thickness. *x* is the porous layer thickness. *d* is the overall film thickness (*x* and *t* are also used to refer to the layers themselves).

homogeneous layers (Figure 6) is proposed here. The innermost layer (closest to the metal substrate) is signified as "*t*" and is compact, while the outer layer, "*x*", is homogeneously porous and permeable to the electrolyte solution. (Note that *x* and *t* are also used herein to signify the thickness of the corresponding layers.) As such, the outer layer forms interconnected pores filled with the electrolyte defining a certain average penetration length. A similar approach was introduced by Ren and Pickup (30) in which the authors consider two different layers exhibiting different electronic and ionic conductivities. This model differs from that proposed herein in that it is based on the differences in the oxidation level of the two layers rather than morphological differences. The frequency-independent impedance behavior observed in our case is not consistent with this particular model.

Our proposed equivalent circuit (Figure 7) for the PEDOT electrode can be described by a hybrid model that combines the transmission line approach with that of an intercalation model (31), thus accounting for both the compact and

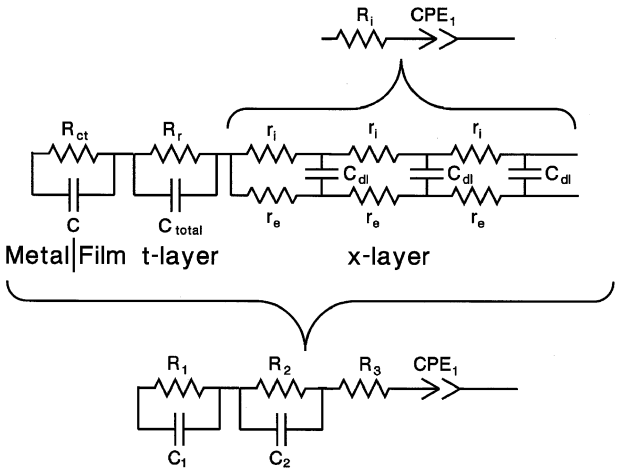

FIGURE 7. Proposed equivalent circuit for a two-layer morphology (PEDOT/BF_4^- electrodes produced using the optimum conditions as defined in this study).

porous layers. Assuming conduction is based on electron (or h^+) transport in the compact layer and ionic transport in the porous layer, the film should exhibit impedance behavior with two different characteristic regimes: one frequency-dependent and one frequency-independent. The point at which there is a transition in impedance from frequency-independent to frequency-dependent behavior is defined by a characteristic frequency, ω_o.

When the perturbation frequency is greater than the characteristic frequency ($\omega \gg \omega_o$), a frequency-independent impedance originating from ohmic ionic resistance in the pore channels is expected (32). Consideration of dual conductivity in the porous layer suggests that charge carriers propagate inward through the pores of the film if the ionic resistance in the electrolyte is lower than that in the polymer mesh. This assumption is supported by the increased porosity and disorder, both of which will decrease intrachain conductivity.

Charge transport in the compact layer proceeds primarily through a fast succession of electron exchange reactions that propagate along the chain in the *t* layer, and the situation where the electronic resistance, R_e, is smaller than ionic resistance, R_i, is assumed (30, 33). As such, the electronic charge carriers move toward the polymer–solution interface. An approximation of the polymer–electrolyte interface as a fractal, more specifically a case of the Koch curve model, as treated by Gols and Geertsman (34) is predicted to result in a constant impedance over a broad frequency because of the double-layer capacitance in the pores. Ions that can still move through the channels will contribute an ohmic solution resistance to the circuit. At a high frequency ($\omega \gg \omega_o$), what would be ordinarily represented by a single charge-carrier-type transmission line representing distributed ionic resistance and capacitance can be reduced to a resistor, R_i, in series with a constant phase element (CPE) that exhibits resistive behavior. The capacitive behavior resulting from the CPE is only observed at low frequencies.

In the low-frequency regime, a scenario where $\omega \ll \omega_o$, the series CPE1 corresponding to the capacitive charging/discharging at the *x*–*t* layer interface becomes dominant. A CPE is utilized for this component because it is not a cleanly defined interface as mentioned above. That is, this interface and associated double-layer charging cannot be defined in terms of the well-known Gouy–Chapman–Stern model of the double layer. It is important to mention that our model ignores counterion diffusion within the more compact film layers based on the assumption that ion transport is too slow to have a noticeable impact on the impedance response. It is reasonable to connect this CPE1 element in series to the rest of the circuit because, before the ions can reach the *t* layer, they must travel through interconnected pore channels. The frequency at which this CPE begins to impact the impedance behavior of the film depends on the ion penetration depth, also determined by the thickness of the *x* layer.

It may seem unrealistic to assume a double-layer charging/discharging within the porous layer of the polymer matrix. However, on the basis of our proposed morphological model, there has to be an ion-blocking layer within the polymer where the charge separation (of opposite signs) will form. It is arguably reasonable to assume some sort of transition layer between the electronic (compact) and ionic (porous) layer. This transition layer is likely to exhibit a dual conductivity characterized by relatively equal ionic and electronic (or h^+) mobility. Regarding this layer as an extension of the *x* layer in our model is consistent with the rigorous theoretical treatment of impedance characteristics of such a structure by Vorontyntsev (35) and co-workers.

The final portion of the proposed circuit includes two parallel RC circuits, one of which represents the electronic charge transfer resistance, R_e, and interfacial capacitance at the polymer–metal film interface and the second of which represents the conduction in the compact *t* layer.

The majority of counterions in the *t* layer are essentially trapped, and the diffusional contribution of these charge carriers to the total impedance is negligible due to the large energy barrier for transport caused by their spatial confinement. Theoretically, the *t* layer should be modeled by an R_rC_{total} circuit, where R_r represents the electronic resistance and C_{total} the capacitive charging caused by trapped counterions. However, this capacitive contribution will be significantly smaller than those of C1 or CPE1, thus obscuring any effect on the total impedance.

This very general circuit can produce a variety of Z''/Z' relationships. Theoretically, it should exhibit two semicircles. Depending on the values of the component elements resulting from the film's microstructure (as described above), the semicircles may not be observed in the frequency range probed. In the case of a film with two different morphologies in series, this equivalent circuit approaches the behavior of a resistor in series with a capacitor or CPE (at a low frequency). At high and medium frequencies, however, an ohmic resistance (50–100 Ω, approximately that of the ionic solution), should be observed. In accordance with the proposed circuit, these electrodes exhibit ohmic behavior that

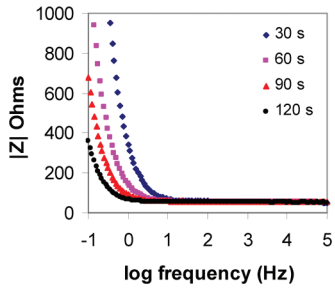

FIGURE 8. Bode plots for electrodes prepared with varying electropolymerization times of (a) 30, (b) 60, (c) 90, and (d) 120 s. The EDOT monomer and tetrafluoroborate concentrations were 0.0125 and 0.1 M, respectively, during polymerization.

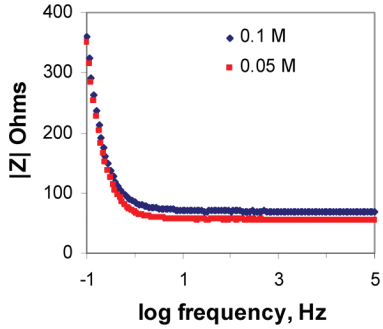

FIGURE 9. Bode plots for electrodes prepared with varying $TBABF_4$ dopant concentrations of (a) 0.1 and (b) 0.05 M. The monomer concentration was 0.0125 M EDOT, and the electropolymerization time was 60 s.

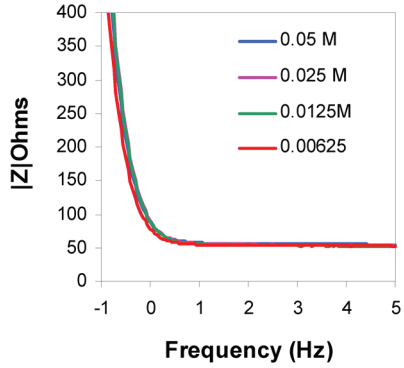

FIGURE 10. Bode plots for electrodes prepared with varying monomer concentrations. The counterion concentration during electropolymerization was 0.1 M BF_4^-, and the electropolymerization time (at $V = 1.2$ V vs Ag/AgCl) was 120 s.

spans almost the entire frequency range probed. Figures 8−10 show that at low frequencies (<10 Hz), the well-known capacitive slope originating from the CPE1 discussed above is observed.

The macrostructural features of the film appear to be responsible for the approach to ohmicity in this frequency range. The mechanism includes injection of electronic (or h^+) charge carriers from the metal into the polymer chains near the metal substrate with transport of those carriers through the film. This model is supported by the results of variations in deposition time, electropolymerization dopant concentration, and monomer concentration described in the next three subsections.

Effect of Deposition Time. It was noted in the discussion of the SEM results that the film porosity increases with electrodeposition time (Figure 5). In theory, longer deposition times should result in a thicker porous layer. However, as more polymer is deposited on the outer layer, it is possible that the monomer and oligomers penetrate or become trapped within the inner layer, subsequently polymerizing to fill in the innermost pores. In this case, a proportional growth of the compact layer and porous layer would occur, causing the frequency window for ohmic behavior to remain the same.

The optimal deposition time is guided by the balance between achieving ohmic behavior within a wider frequency and achieving good mechanical properties of the film. While a shorter deposition time (<30 s) results in a film that exhibits largely capacitive impedance ($C = 40\ \mu F/cm^2$ at 0.1 Hz), a deposition time of >120 s results in thick, porous, and brittle films. The fragility of the film may be caused by large voids (gaps between polymer strands) that may form, decreasing the number of interchain contacts. The capacitive behavior of the thinner film (electropolymerization time of ≤30 s) is consistent with what would be expected when the porous layer is absent, in which case the surface would be considered as rough instead of porous. It is also possible that a short polymerization time led to incomplete coverage of the underlying substrate electrode.

Figure 8 compares the Bode plots of electrodes produced using different deposition times. It is obvious that the ohmic resistance is almost the same (see $|Z|$ values) in the high-, intermediate-, and moderately low-frequency ranges. However, it is also observed that impedance of thinner films (short electropolymerization time) deviates from ohmic behavior before that of thicker films. Thin films exhibit higher capacitances at low frequencies than thick films as a consequence of their smoother morphology. Assuming that the compact layer exhibits good electronic conductivity and spatially limited ionic diffusion, impedance of a very thin film would be mainly determined by the double-layer capacitance in medium- and low-frequency ranges.

Effect of Dopant Concentration. With increased solution conductivity, the rate of nucleation and growth of the film on the electrode surface is likely to be faster, leading to a less structured t layer containing random polymer aggregates and increasing the $|Z|$ value as seen in Figure 9. The anions have also been implicated in inhibition effects on the oxidation of the monomer onto the electrode surface when it is less concentrated than the dopants (36). Blocking the nucleation sites could result in a less structured first layer and inhomogeneous growth. An alternative interpretation of this high impedance hinges on the ionic and electronic (or h^+) charge carrier interaction. It is generally agreed that anions can act as binding sites that immobilize the charge carriers with opposite charge (26). Although increasing the concentration of dopants in the solution does not translate into the incorporation of counterions into the film under normal circumstances, some counterions may be trapped in the compact layer. These

would hinder the hopping of positive charge from one site to the neighboring site. This is consistent with the slightly increased electronic resistance that can be assigned to hole/electron transport in the compact layer. Furthermore, the inclusion of more counterions would be expected to contribute to structural deformation, particularly in the *t* layer, and lead to limited interchain transport and observable ionic diffusion transport. Therefore, the suggested explanation of higher impedance at higher counterion concentrations is based primarily on the contribution of the counterion's effects on structure disorder of the compact layer and associated hindered electronic transport.

Effect of Monomer Concentration. Higher concentrations of the monomer also should lead to faster initial polymerization rates at the surface of the electrode. This faster deposition rate would be expected to result in a less ordered, less compact, layer adjacent to the surface for a given total charge passed (in other words, would decrease the *t* layer thickness). While crystalline regions are highly conductive, the disordered regions will act as insulator islands due both to the absence of π wave function overlap and, even where overlap is maintained, to Peierls distortion (37). The impedance also would increase not only because this layer is no longer blocking to the electrolyte but also because this more porous *t* layer would be characterized by smaller noninterconnected voids. Furthermore, in such a model, the influence of ionic conductivity is more pronounced. This is consistent with the experimental results for 0.05, 0.025, and 0.0125 M monomer deposition solutions shown in Figure 10. The impedance modulus at a given frequency increases with a higher monomer concentration because of the disorder introduced during the fast polymerization. As in the case of electrodes produced at higher counterion concentrations, these conditions (increased monomer concentration) shorten the frequency range within which ohmic behavior is observed. Electrodes prepared using a lower monomer concentration (0.0125 M EDOT), on the other hand, exhibit lower impedance and ohmic behavior within a larger frequency range. The higher impedance in the case of the 0.00625 M monomer case would appear to be a result of the fact that the monomer concentration has, at this point, reached a value where the rate of production of a sufficient oligomer is insufficient for the nucleation and growth necessary to produce the required two-layer morphology. It is also important to highlight the fact that at very low frequencies, all films made at different concentrations appear to exhibit the same low-capacitive frequency impedance behavior. These observations suggest that the charging mechanism is the same for these films and is largely determined by the double-layer charging that takes place inside the pores of the film.

Effect of Deposition Mode. PEDOT films may be produced using potentiostatic, galvanostatic, coulostatic, or cyclic voltammetric deposition. As shown in Figure 11, the impedance behavior is similar for all of these approaches. However, potentiostatic deposition has been chosen as it provides a facile, reproducible method and a slightly improved range over which the desired frequency-independent behavior is obtained (phase angle of <2°). It is worth noting, however, that optimization of solution composition parameters while using a different mode may well result in a broader range.

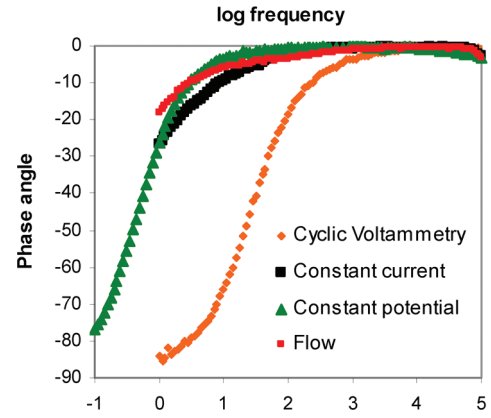

FIGURE 11. Comparison of behavior using different deposition modes at 0.0125 M EDOT and 0.1 M TBATFB. For constant potential and flow methods, $V = 1.3$ V vs Ag/AgCl. For the CV method, potential limits of 0 and 1.35 V vs Ag/AgCl were used (20 cycles). For a constant current, $i = 1$ μA/cm^2.

Comparison of Model and Experimental Impedance Behavior. The extent of agreement between the model proposed above and experimental results is also borne out by comparison of calculated impedance data and that for an electrode prepared using the optimized parameters discussed here. As seen in Figure 12, the simulated and experimental data show

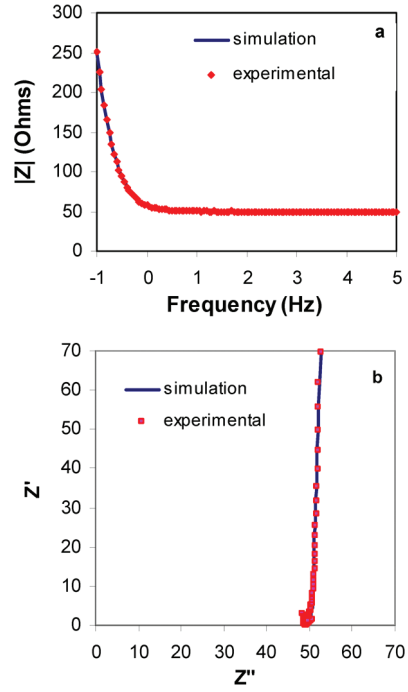

FIGURE 12. Comparison of theoretical behavior of a circuit with that of an electrode produced using optimal conditions: (a) experimental and (b) theoretical fit. Fitting parameters: $R_1 = 3.4$ Ω, $R_2 = 3.8$ Ω, $R_3 = 38.1$ Ω. CPE1: CPE-$T = 0.00879$, CPT-$P = 0.977$F; $C_1 = 0.042$ F, $C_2 = 2.7 \times 10^{-7}$ F.

Table 2. Fitting Parameters for the Proposed Model ($N = 6$)

parameter	mean	s
R_1 (Ω)	1.4	0.2
C_2 (F)	6.2×10^{-6}	2.8×10^{-6}
C_1 (F)	0.0008	0.0001
R_2 (Ω)	3.3	0.7
R_3 (Ω)	49	3
CPE1-T	0.0012	0.0002
CPE1-P	0.992	0.002

excellent agreement over the range probed for both Bode and Nyquist representations of the data. Values are given in Table 2 for a set of six electrodes prepared using the optimized deposition parameters and are a measure of the reproducibility of the method.

Because R_1 represents the resistance of the back junction, it is not unexpected that the value for this parameter is low. This is likely to be due to the intimate contact formed between the film and the electrodeposited gold layer before formation of the compact, homogeneous layer described in the text. During electrode polarization, the charge carriers are localized at the surface of the imperfections in the gold surface, allowing facile charge transfer into the polymer chains.

Although EIS is generally not performed on cylindrical (wire) electrodes, we have confirmed that the same frequency-independent behavior is obtained at disk electrodes (Figure 13). Differences in the fitting parameters can be justified as a function of the surface area of the electrode.

4. CONCLUSIONS

Conditions for the consistent production of conducting polymer films employing potentiostatic deposition at 1.3 V for 60−90 s have been determined. The optimal concentration of the monomer is 0.0125 M, and that of the counterion is 0.05 M. EIS data indicate that ohmic behavior is consistently achieved under these conditions from ∼10 Hz to 50 kHz. The small random deviation from zero in the phase angle and from an average impedance modulus over this range indicates minimal reactive impedance within this frequency range. The small deviation from a perfect resistor may be caused by the back junction and/or small differences in polymer film homogeneity. When fabricated using the optimal conditions reported here, the high-frequency impedance modulus and the low-frequency cutoff for constant, non-frequency-dependent impedance (phase angle of less than ±2°) were both consistent electrode to electrode. The results of these studies imply that nonionic (i.e., electron or h^+) charge transport is the rate-limiting factor in this high-frequency range in contrast to that at very low frequencies.

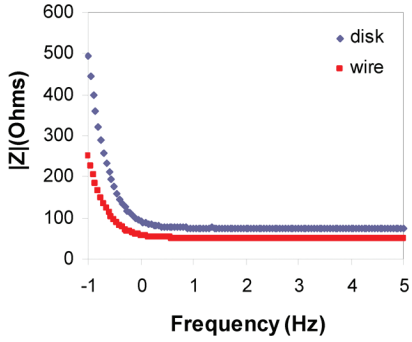

FIGURE 13. Example of disk vs wire electrode behavior at 0.0125 M EDOT and 0.1 M TBATFB. $V = 1.3$ V vs Ag/AgCl, and $t_{dep} = 120$ s.

The proposed model, which relies on a two-regime polymer film, is consistent with EIS data for films produced under a variety of polymerization conditions.

Acknowledgment. J.F.R. and Y.P.K. express their appreciation for the Department of Chemistry and the Graduate School of Arts and Sciences of Georgetown University for their financial support. Y.P.K. also acknowledges the support of the Bou Foundation. In addition, the authors express their appreciation to J. Ross McDonald and K. A. Rubinson for helpful discussion and to a number of undergraduate students at Georgetown University who contributed to the work presented here, including Michael Flaherty, Danielle Howard, and Sarika Agrawal.

REFERENCES AND NOTES

(1) Ovadia, M.; Fayn, E.; Zavitz, D. H. *Chem. Phys. Lett.* **2006**, *424*, 285–288.
(2) Chou, H.; Ovadia, M.; Moskowitz, M.; Zavitz, D. *PACE, Pacing Clinical Electrophysiology* **2000**, *23*, 386–394.
(3) Ovadia, M.; Zavitz, D. *Chem. Phys. Lett.* **2004**, *390*, 445–453.
(4) Asplund, M.; Thaning, E.; Lundberg, J.; Sandberg-Nordqvist, A. C.; Kostyszyn, B.; Inganas, O.; von Holst, H. *Biomed. Mater.* **2009**, 045009.
(5) Fonner, J. M.; Forcinilli, L.; Nguyen, H.; Byrne, J. D.; Kou, Y.-F.; Syeda-Nawaz, J.; Schmidt, C. E. *Biomed. Mater.* **2008**; 034124.
(6) Luo, S.-C.; Ali, E.; Tansil, N.; Yu, H.-H.; Gao, S.; Kantchev, E.; Ying, J. *Langmuir* **2008**, *24*, 8071–8077.
(7) Dietrich, M.; Heinze, J.; Heywang, G.; Jonas, F. *J. Electroanal. Chem.* **1994**, *369*, 87–92.
(8) Yamato, H.; Ohwa, M.; Wernet, W. *J. Electroanal. Chem.* **1995**, *397*, 163–170.
(9) Bobacka, J.; Lewenstam, A.; Ivaska, A. *J. Electroanal. Chem.* **2000**, *489*, 17–27.
(10) Cogan, S. *Annu. Rev. Biomed. Eng.* **2008**, *10*, 275–309.
(11) Richardot, A.; McAdams, E. T. *IEEE Trans. Med. Imaging* **2002**, *21*, 604–612.
(12) Nardes, A. M.; Kemerink, M.; Janssen, R. A. J.; Bastiaansen, A. M.; Kiggen, N. M. M.; Langeveld, B. M. W.; van Breeman, A. J. J. M.; Kok, M. M. d. *Adv. Mater.* **2007**, *19*, 1196–1200.
(13) Cui, X.; Martin, D. C. *Sens. Actuators, A* **2003**, *103*, 384–394.
(14) Xiao, Y.; Cui, X.; Martin, D. C. *J. Electroanal. Chem.* **2004**, *573*, 43–48.
(15) Ovadia, M.; Zavitz, D. H.; Rubinson, J. F.; Park, D.; Chou, H. A. *Chem. Phys. Lett.* **2006**, *419*, 277–287.
(16) Kaynak, A. *Mater. Res. Bull.* **1997**, *32*, 271–285.
(17) Sweeney, C. T.; Forcelli, P.; Kammerich, A.; Lee, B. C.-W.; Gale, K. N.; Rubinson, J. F. Manuscript in preparation.
(18) Kammerich, A.; Srivastava, Y.; Hargett, K.; Harrison, V.; Rubinson, J. *J. Electrochem. Soc.* **2009**, *156*, P68–P73.
(19) Beck, F.; Michaelis, R. *J. Coat. Technol.* **1992**, 64.
(20) Zykwinska, A.; Domagala, W.; Pilawa, B.; Lapkowski, M. *Electrochim. Acta* **2005**, *50*, 1625–1633.
(21) Eliseeva, S.; Spiridonova, D.; Tolstopyatova, E.; Kondratiev, V. *Russ. J. Electrochem.* **2008**, *44*, 894–900.
(22) Chiu, W.; Travas-Sedjic, J.; Cooney, R.; Bowmaker, G. A. *J. Raman Spectrosc.* **2006**, *37*, 1354–1361.
(23) Chiu, W. W.; Travas-Sejdic, J.; Cooney, R. P.; Bowmaker, G. A. *Synth. Met.* **2005**, *155*, 80–88.
(24) Casado, J.; Zotti, G.; Berlin, A.; Hernandez, V.; Ortiz, R.; Navarrete, J. *J. Mol. Struct.* **2005**, *744−747*, 551–556.

(25) Laforgue, A.; Robitaille, L. *Macromolecules* **2010**, *43*, 4194–4200.
(26) Reghu, M.; Subramanyam, S. V.; Chatterjee, S. *Phys. Rev. B* **1991**, *43*, 4236.
(27) Kemp, N. T.; Cochrane, J. W.; Newbury, R. *Synth. Met.* **2009**, *159*, 435–444.
(28) Soto, J. P.; Díaz, F. R.; del Valle, M. A.; Vélez, J. H.; East, G. A. *Appl. Surf. Sci.* **2008**, *254*, 3489–3496.
(29) Kupila, E.-L.; Kankare, J. *Synth. Met.* **1995**, *74*, 241–249.
(30) Ren, X.; Pickup, P. G. *J. Electroanal. Chem.* **1997**, *420*, 251–257.
(31) Bisquert, J. *Electrochim. Acta* **2002**, *47*, 2435–2449.
(32) Rossberg, K.; Paasch, G.; Dunsch, L.; Ludwig, S. *J. Electroanal. Chem.* **1998**, *443*, 49–62.
(33) Albery, W. J.; Mount, A. R. *J. Chem. Soc., Faraday Trans.* **1994**, *90*, 1115–1119.
(34) Gols, J. E.; Geertsma, W. *J. Phys.: Condens. Matter* **1989**, 4469.
(35) Vorotyntsev, M. A.; Daikhin, L. I.; Levi, M. D. *J. Electroanal. Chem.* **1994**, *364*, 37–49.
(36) González-Tejera, M. J.; Carrillo, I.; Hernández-Fuentes, I. *Synth. Met.* **1998**, *92*, 187–195.
(37) Heeger, A. *J. Phys. Chem. B* **2001**, *105*, 8475–8491.
(38) Jow, T. R.; Xu, D.; Deng, S. P. Vol. DOE/ID/13451, p 17, U.S. Department of Energy: Washington, DC, 1999.

AM100480S